

Droplet Morphology and Mobility on Lubricant-Impregnated Surfaces: A Molecular Dynamics Study

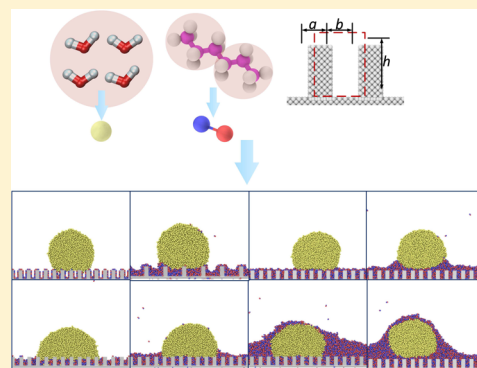
Lin Guo,^{†,‡} G. H. Tang,^{*,†,‡} and Satish Kumar^{*,‡}

[†]MOE Key Laboratory of Thermo-Fluid Science and Engineering, School of Energy and Power Engineering, Xi'an Jiaotong University, Xi'an 710049, P.R. China

[‡]G. W. Woodruff School of Mechanical Engineering, Georgia Institute of Technology, Atlanta, Georgia 30332, United States

Supporting Information

ABSTRACT: Slippery liquid-infused porous surfaces (SLIPS) are gaining remarkable attention and have advanced performance in many fields. Although all SLIPS are related to lubricant-impregnation within nano/microstructures on a surface, they differ in many aspects, such as the morphology of droplets, the state of cloaking, the wetting edge, and the lubricant thickness. Requirements of the droplet morphology on SLIPS might change according to a specific application. A molecular-dynamics-based numerical model that can correctly simulate SLIPS is developed and is validated by comparing against the theoretical predictions for all possible stable states for a given droplet, lubricant, and solid surface. On the basis of this model, a detailed analysis of the equilibrium states is conducted. In particular, we discover that the four possible stable states on SLIPS predicted by theoretical studies can be extended to eight states by considering the effects of lubricant thickness and surface geometry in addition to the interfacial tension and surface wettability. These findings could be used to determine the conditions under which a thermodynamically stable state exists on SLIPS. The dynamic behavior of a nanodroplet on SLIPS is also studied, which provides insight into how a proper increase in the lubricant thickness might increase the sliding velocity. The above findings and developed model are expected to provide significant guidelines for designing SLIPS.



INTRODUCTION

The *Nepenthes* pitcher plant has been reported to have an extremely slippery surface by forming a layer of nectar or water on its roughed surface to capture insects.^{1–4} Inspired by the pitcher plant, Aizenberg et al.⁵ developed a novel surface named slippery liquid-infused porous surfaces (SLIPS). The liquid is trapped in the pores of the rough surface by capillarity, forming a smooth and homogeneous surface on which the contact angle hysteresis is extremely small.^{6–8} In addition to the low contact angle hysteresis, SLIPS also exhibit antiwetting behavior to almost all fluids and show extreme temperature and pressure stability. With these remarkable properties, SLIPS have been reported to have advanced performance in fields such as condensation,^{9–16} antifouling,^{17–23} anti-icing,^{24–27} antifrosting,^{28,29} bubble transportation,^{30,31} solar energy harvesting,³² and anticell proliferation.³³ SLIPS have been successfully fabricated using UV lithography,^{12,34,35} electrodeposition,²⁴ hydrothermal treatment,^{36,37} non-solvent-induced phase separation,³⁸ solution blow spinning,³⁹ acid etching,⁴⁰ and hydrophobized nanoparticle deposition.⁴¹

Various types of oils have been chosen as lubricants and deposited on substrates with different types of material to fabricate SLIPS. These surfaces were all lubricant-impregnated with an extremely small water droplet sliding angle. However, these SLIPS differ in many aspects, such as the morphology of

droplets, the state of cloaking, the wetting edge, and the lubricant thickness. Thus, SLIPS with different parameters might have different performances when applied to different fields. For example, the cloaking of condensed water drops may adversely affect condensation heat transfer and decrease the longevity of the coating by displacing the lubricant,⁴² while the bubble transportation will be more stable with wrapped-around lubricant.³¹ The wetting ridge is important and influences the viscous dissipation in a mobile drop and merging droplets.⁴³ Furthermore, for application under a specific condition, preferred parameters such as the lubricant thickness might be different and need exploration to find the optimal value. An excess oil film may be beneficial to reducing ice adhesion, but the excess lubricant is not stabilized by capillary forces and can be readily drained by gravity and other forces.^{43,44} Therefore, it is of great significance to explore the principles underlying SLIPS.

There have been some experimental and theoretical studies about the principles of SLIPS. Anand et al.⁹ and Kajiyama et al.⁴⁵ performed experiments to study condensate droplet morphologies on lubricant-impregnated surfaces with different types of lubricants. Smith et al. described the thermodynamics of drops

Received: August 19, 2019

Revised: October 30, 2019

Published: November 8, 2019

on lubricant-impregnated surfaces and showed that a drop on a lubricant-impregnated surface can exist in 1 of 12 different thermodynamic states depending on the properties of the working fluid droplet, impregnating lubricant, solid texture, and surrounding environment.³⁵ You et al. emphasized that any solvents with surface tension greater than that of the lubricant are able to repel the infused lubricant, and droplet directional motion was realized on the basis of this phenomenon.⁴⁶ Guan et al. theoretically and experimentally studied the diffusion-limited evaporation of droplets on lubricated textured surfaces.⁴⁷ Schellenberger et al. analyzed the wetting ridge of several lubricant-impregnated surfaces and found that the height of the wetting ridge follows a balance between Laplace pressure and hydrostatic pressure.⁴³ Wang et al. studied the lubricant thickness effect on the surface roughness during bacterial and algae settlement analysis.³⁷ Kreder et al. studied the film dynamics and lubricant depletion on lubricated surfaces.⁸

It is reasonable to analyze the morphology of the working fluid droplet on SLIPS using theoretical and experimental techniques. While investigating the details for a specific application, it is difficult to analyze or observe droplet morphology directly. For example, while exploring condensation, it is hard to directly observe nucleation sites of the condensed droplets on the SLIPS, which is needed to elucidate heat transfer. It is also difficult to control the lubricant thickness and observe the droplet state at small scales using experimental methods. Therefore, it is necessary to develop numerical methods to simulate the governing principles on SLIPS on the basis of which further simulations of specific conditions can also be performed.

There are four important factors for SLIPS: the working fluid, the lubricant, the substrate, and the working conditions. This makes the analysis complicated. A computational framework for the rapid analysis of such systems has not yet been developed. For the investigation of surface wettability, many computational studies have been performed on the superhydrophobic surfaces, which is a relatively simple system with two components. Molecular dynamics simulations have been used in these investigations to evaluate the wettability of various surfaces.^{48–52} Ramos-Alvarado et al. studied the wettability of graphitic carbon and silicon surfaces using the molecular dynamics model.⁴⁸ Li et al. arranged nanostructures on a copper surface to resemble the macroscopic rough surface with nanopillars and obtained a superhydrophobic surface with a low surface free energy.⁵⁰ Niu et al. simulated the contact angle of water nanodroplets on the platinum surface. By changing the energy parameters between water molecular and the platinum atom, different wettabilities from hydrophilic to hydrophobic were realized.⁵¹ Inspired by these molecular dynamics simulations, we developed a numerical model of the lubricant-impregnated surface by adding a third component (i.e., the lubricant). This model can correctly predict the morphology of droplets and explain the predictions by theory or experiments. Apart from the equilibrium state of this four-component system, we also investigate the dynamic behavior and study the sliding angle of the droplets on SLIPS. The effects of the lubricant–water interfacial tension, the lubricant thickness, the surface wettability, and the roughness structure have also been studied using the developed numerical model. There have been few computational studies on the lubricant-impregnated surface. It is expected that the method presented in this work will provide guidelines for designing SLIPS and help in better explaining future experimental and theoretical observations.

NUMERICAL METHODOLOGY

Molecular dynamics simulation was performed using the large-scale atomic/molecular massively parallel simulator (LAMMPS) package. Water is picked as the working fluid, and copper, as the solid substrate. Typical lubricants used in the experiments are fluorocarbons (e.g., Krytox, FC-70), fatty alcohols (e.g., decanol), hydrocarbons, silicone oils, and ionic liquids (e.g., BMIM). The molecular structures of these lubricants are very complicated, which requires large computational sources. For simplicity, we chose hexane with a very simple structure among *n*-alkanes as the lubricant. We show that the hexanelike structure can be correctly simulated, and the morphology under different conditions can be reasonably predicted on the SLIPS.

To reduce the computational cost and extend the time and length scales compared to the all-atom model, we apply a coarse-grained model for water molecules and hexane molecules developed by Chiu et al.⁵³ This model has been successfully adapted for both highly polar (water) and nonpolar (alkanes) species. A coarse-grained bead is applied to represent four water molecules, indicated as W in Figure 1. The hexane bead consists of two particles, and each particle contains three CH₂/CH₃ groups, which is represented by CT. The Morse potential is used for particle–particle interactions of water and hexane, which has the form⁵³

$$E_{\text{water-water, hexane-hexane}} = D_0 [e^{-2\alpha(r-r_0)} - 2e^{-\alpha(r-r_0)}] r < r_c \quad (1)$$

where r_c is the cutoff.

The Lennard-Jones potential is used for the water and hexane interactions, which can be given by⁵⁴

$$E_{\text{water-hexane}} = \frac{3\sqrt{3}}{2} \epsilon \left[\left(\frac{\sigma}{r} \right)^{12} - \left(\frac{\sigma}{r} \right)^6 \right] r < r_c \quad (2)$$

σ for two different particles is calculated by the arithmetic average following Lorentz–Berthelot mixing rules. σ_w equals 0.47 nm⁵⁵ and σ_{CT} equals 0.45850 nm,⁵⁴ so σ equals 0.4642 nm. By changing ϵ , we can get different interfacial tensions between water and hexane.

We choose copper atoms to build the solid surface with nanocolumns arranged on the surface. The geometry parameters of nanostructures are shown in Figure 1c, where $a = 14.4596 \text{ \AA}$, $b = 17.3515 \text{ \AA}$, and $h = 32.5341 \text{ \AA}$. The copper atoms are fixed by setting the velocities to zero and the restricting force acting on them to zero. The standard 12/6 Lennard-Jones potential is used for the interaction of copper/water, copper/hexane, and copper/copper, given by⁴⁹

$$E_{\text{water-solid, hexane-solid, copper-copper}} = 4\epsilon \left[\left(\frac{\sigma}{r} \right)^{12} - \left(\frac{\sigma}{r} \right)^6 \right] r < r_c \quad (3)$$

where the LJ parameters of copper, ϵ_{Cu-Cu} and σ_{Cu-Cu} from ref 49 are employed in the present work. By changing ϵ , we can get different wettabilities for water and hexane.

The potential used for the simulations and their parameters are summarized in Table 1.

The simulations can be categorized into four parts:

(1) Simulation of the Interfacial Tension and Fluid Density. First, the surface tension of water and hexane and the interfacial tension between water and hexane are calculated and compared with the experimental results. The starting config-

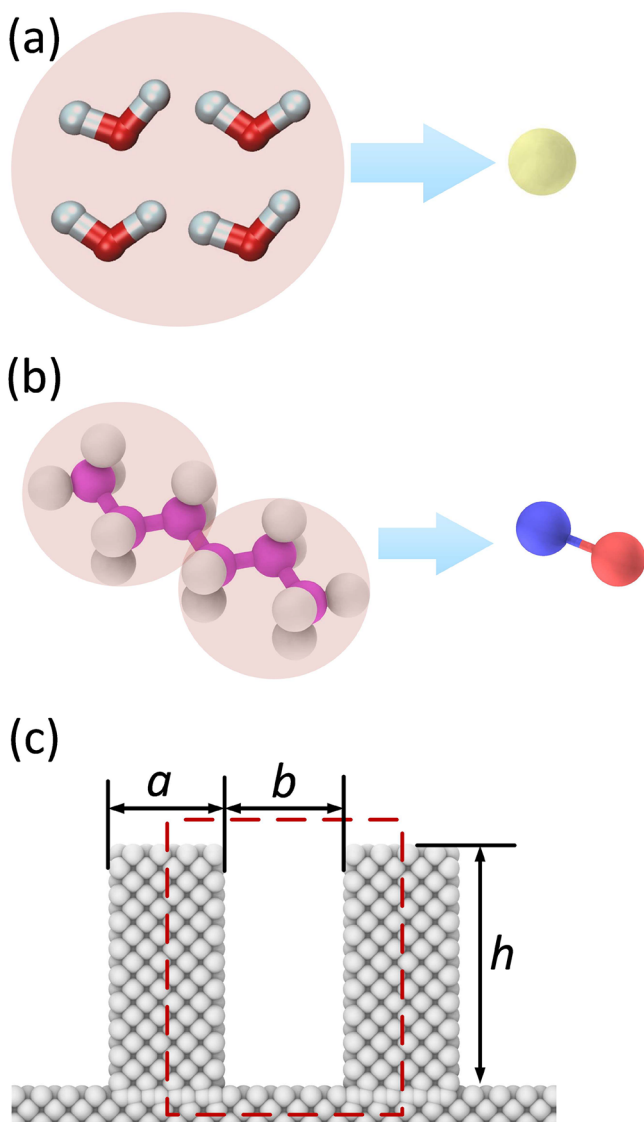


Figure 1. Schematic diagram of (a) the water bead, (b) the hexane bead, and (c) the nanostructure configuration on a copper surface; a refers to the nanocolumn width, b refers to the nanocolumn spacing, and h refers to the nanocolumn height.

Table 1. Potential Parameters

interaction site	potential	corresponding parameters			
		D_0 [kcal/mol]	α [\AA^{-1}]	r_0 [\AA]	r_c [\AA]
W-W	Morse	0.813	0.556	6.29	16
CT-CT	Morse	0.703	1.139	5.27	16
interaction site	potential	ϵ [kcal/mol]	σ [\AA]	r_c [\AA]	
Cu-Cu	12/6 LJ	4.72	2.616	13	
W-Cu	12/6 LJ		3.658	13	
CT-Cu	12/6 LJ		3.601	13	
interaction site	potential	ϵ [kcal/mol]	σ [\AA]	r_c [\AA]	
W-CT	12/4 LJ		4.642	15	

urations are shown in Figure S1. The total length in the x and z directions of the simulation box are set as 50 \AA , and the length in the y direction is set as 150 \AA for all three cases. Lattice structures of face-centered cubic (FCC) unit cells are employed to model the water with a lattice constant of 8 \AA . Water beads (1098 and 2028) are considered in the simulations corresponding to the

results shown in Figure S1a,c, respectively. Before generating hexane beads in the simulation box, one hexane bead is defined first. The bond type is harmonic with coefficient $K = 5.9725 \text{ kcal}\cdot\text{mol}^{-1} \text{ \AA}^{-2}$, and the bond length is 3.6 \AA . Then 594 hexane beads are generated in a $50 \times 50 \times 50 \text{ \AA}^3$ domain, as shown in Figure S1b,c. The periodic boundary condition is applied to all three directions. The MD simulations in NPT are carried out for 1 ns to attain equilibrium and are run for 1 ns to collect the surface tension data along with time.

The surface tension γ is calculated by⁵⁴

$$\gamma = \frac{L_x}{2} \left(P_{xx} - \frac{P_{zz} + P_{yy}}{2} \right) \quad (4)$$

where the factor of $1/2$ is included to account for the two interfaces in the simulation box, P_{ij} is the ij component of the averaged pressure tensor, and L_x is the box size in the x direction.

(2) Simulation of the Contact Angle of Water/Hexane on the Copper Surface. The wettability of water on copper and hexane on copper is investigated using the cylindrical droplet method to get rid of the effect of the line tension.^{48,56} The computation box is $510 \times 546 \times 994 \text{ \AA}^3$ in length. A periodic boundary condition is imposed in the three directions of the computational domain. There are 3023 water beads and 480 hexane beads for calculations of water and hexane contact angles in air, and 480 hexane beads and 4620 water beads are used in the computation of the hexane contact angle in the water.

At first, a water box or a hexane box with perfectly arranged beads is placed at a prudent distance on top of a solid surface, and the system is allowed to equilibrate. The initial configurations are shown in Figure S2. Energy minimization of the system is conducted to remove any excess potential energy from the initial configuration. Then the system is equilibrated using a Nose/Hoover thermostat at 303 K with a time constant of 10 fs for 0.5 ns. After that, equilibration in the microcanonical ensemble with a time step of 10 fs for 0.5 ns is conducted, and snapshots of the system are collected for the next 3 ns.

To extract the profile of the contact line, cylindrical liquid slabs are equilibrated over atomically flat surfaces, and the solid surface is assumed to be straight. Then the microscopic contact angle is considered to be similar to its macroscopic counterpart as predicted by the modified Young's equation. The contact angle calculation procedure is as follows: (a) The computational box is discretized into bins of square cross sections in the x - y plane, and the entire length of the computational box in the z direction is considered to be the depth of the bins. The resolution of the bins was set as $0.8 \times 0.8 \text{ \AA}^2$. The position of each atom of the tested group is stored in the appropriate bin for every snapshot, and the mass density is calculated as the average over time of the bins count per unit volume. (b) The averaged mass density of bins is plotted as contour maps, and the droplet interface is defined by the contour line in which $\rho(x, y) = \rho_l/2$, where ρ_l is the fluid density. (c) The coordinates of the surface position and the droplet interface are obtained and fitted using the equation of a circle. (d) Finally, the fitted equation is plotted, and the contact angle is measured.

(3) Simulation of the Water–Hexane–Copper System.

To get the morphology of the droplet on SLIPS, four steps are required as shown in Figure S3. The computational box size is $510 \times 546 \times 994 \text{ \AA}^3$, and 3130 water beads are generated for the calculation. The number of hexane beads is changed to get different lubricant thicknesses. The periodic boundary condition

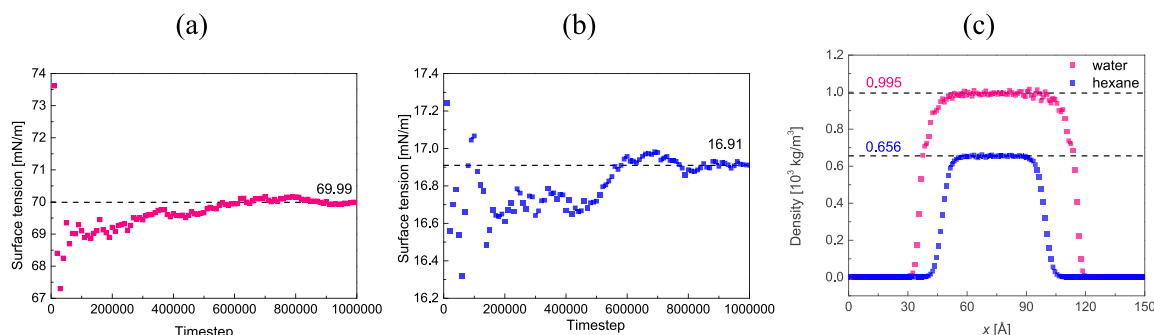


Figure 2. (a) Surface tension of water with time. (b) Surface tension of hexane with time. (c) Density of water and hexane in the x direction.

is applied to all three directions. The simulation process is as follows: (a) First, the hexane beads are put on the solid surface with nanostructures (Figure S3a) and equilibrated at 303 K using a Nose/Hoover thermostat with a time step of 10 fs for 0.5 ns. The contact angle of the hexane on the surface is extremely small, so hexane beads will fully wet and form a film on the surface, resulting in a lubricant-impregnated surface (Figure S3b). (b) Then the water droplet is added to the lubricant-impregnated surface (Figure S3c) and equilibrated at 303 K using a Nose/Hoover thermostat with a time step of 10 fs for 0.5 ns. (c) The next step is equilibration in the microcanonical ensemble for 0.5 ns. (d) The final step is a production run of 3 ns and a collection of snapshots of the water–hexane–copper system every 0.5 ps, and Figure S3d is shown as an example.

(4) Simulation of the Nanodroplet Sliding Behavior.

To study the nanodroplet sliding behavior, a body force is applied to the droplet after the equilibration. The periodic boundary condition is applied in all three directions. We apply a body force in the positive x direction to the water beads to cause the water to experience a constant acceleration, as shown in Figure S4. Then we study the effect of the body force on the droplet motion behavior.

RESULTS AND DISCUSSION

Verification of Potential Parameters with Experimental Results. The surface tension and density of water and hexane are important properties for the lubricant-impregnated surface. The simulation results of surface tension and density are compared with the experimental data at 303 K for verification. The simulated surface tension and density against time and x coordinate, respectively, are plotted and shown in Figure 2. Computational results are marked as black dashed lines. Experimentally measured surface tensions of water and hexane at 303 K are 71.20 and 17.98 mN/m, respectively, and the densities are 995 and 656 kg/m³, respectively. We can see that the simulation parameters predict the density and the surface tension well.

Energy Parameter Exploration. There are three interfaces in this four-component system: interface A (water–air–oil), interface B (solid–water–oil), and interface C (solid–air–oil), as illustrated in Figure 3. Interface A refers to the interface between water and air, having two possible states: cloaking and not cloaking. The cloaking state means that the water droplet is encapsulated in the lubricant. Interface B refers to the interface underneath the droplet (in a water environment). Depending on whether the droplet will be fully suspended by the lubricant or will be suspended by the lubricant but can touch the solid surface or replace the lubricant, the state of interface B is divided into three categories: encapsulated, emerged, and impaled. Interface

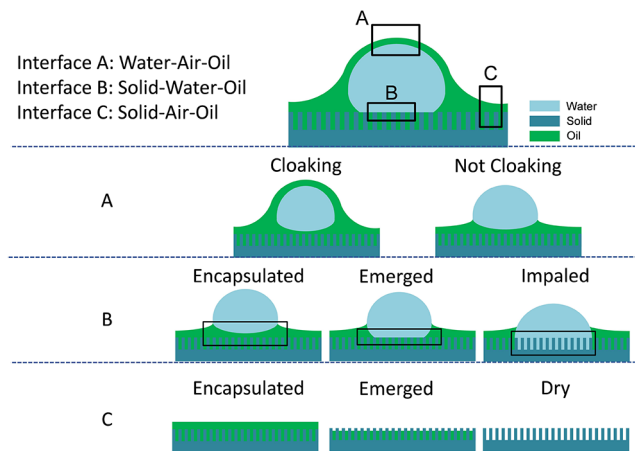


Figure 3. Illustration of the lubricant-impregnated surface. There are three interfaces in this four-component system: (A) water–air–oil, (B) solid–water–oil, and (C) solid–air–oil. Every interface has two (cloaking and not cloaking), three (encapsulated, emerged, and impaled) and three (encapsulated, emerged, and dry) states, respectively.

C refers to the interface outside the droplet (in an air environment). There are three possible configurations for interface C (encapsulated, emerged, and dry), depending on whether the nanostructures will be fully covered by the lubricant or will only be infused in gaps or will not be wetted at all.

The value of the interfacial tension between oil and water can influence the state of interface A. It can be decided whether the cloaking state occurs by determining whether the spreading parameter is larger than 0 or smaller. The cloaking state will occur when the spreading parameter $S_{ow(a)} = \gamma_{wa} - \gamma_{oa} - \gamma_{ow} > 0$, where γ refers to the surface tension, with subscripts o, w, and a representing oil, water, and air, respectively. By changing the energy parameter ϵ_{CT-W} , we are able to obtain both states. Table 2 lists the energy parameter ϵ_{CT-W} used in the present work, corresponding to the results of $S_{os(w)}$, and whether the cloaking state is attained.

States of interface B and C are controlled by the surface wettability. Smith et al. theoretically studied the possible stable

Table 2. Spreading Coefficient

ϵ_{CT-W} [kcal/mol]	γ_{wa} [mN/m]	γ_{oa} [mN/m]	γ_{ow} [mN/m]	$S_{ow(a)}$	cloaking state
0.35	69.66	16.89	60.80	<0	no
0.43	69.66	16.89	48.88	>0	yes
0.60	69.66	16.89	11.07	>0	yes

states for a given droplet, oil, and substrate material on the lubricant-impregnated surface.³⁵ Three equivalent criteria were proposed to classify these states. We choose the contact angle as the criteria in the present work, which is relatively easy and intuitive to analyze. It should be noted that these criteria are equivalent to each other. There are two parameters in contact angle criteria θ : the contact angle of hexane(o) on copper surface(s) in the presence of corresponding air(a) $\theta_{\text{os(a)}}$ and in the presence of water(w) $\theta_{\text{os(w)}}$, different values of which can be achieved by changing energy parameter $\epsilon_{\text{CT-Cu}}$ and $\epsilon_{\text{W-Cu}}$. According to the surface geometry parameters, the critical angle θ_c can be calculated from $\cos \theta_c = (\varphi_s - 1)/(r - \varphi_s)$, where $\varphi_s = a^2/(a + b)^2$, and $r = 1 + 4ab/(a + b)^2$.⁵⁷ Therefore, the critical angle θ_c equals 107.5° in the present case. To fulfill the requirement of $\theta_{\text{os(a)}}$ and $\theta_{\text{os(w)}}$, various value combinations are tested. The chosen values are presented in Table 3 with the hexane contact angle profile under every criterion shown in Figure S5.

Configurations of Droplets on Lubricant-Impregnated Surfaces. With the parameters explored in Table 3, we are able to simulate all of the possible states of these three interfaces. There are 18 combinations in total, and the corresponding morphologies in equilibrium states are shown in Figure 4. The numbers of hexane beads remains 385.

It should be noted first that a stable lubricant-impregnated state will not form on the solid surface if $\theta_{\text{os(a)}} > \theta_c$ for the reason that the lubricant will not wet the solid surface, which is represented as the no impregnation areas in Figure 4. Thus, 12 stable states are left and divided into 2 large columns according to the value of the spreading coefficient. When $\epsilon_{\text{CT-W}} = 0.43$ kcal/mol, droplets in the six subclasses will be in the cloaking states because the spreading coefficients are larger than zero (Table 2). In contrast, not all droplets in the subclasses will be wrapped by the lubricant when $\epsilon_{\text{CT-W}} = 0.35$ kcal/mol, in which case the spreading coefficients are smaller than zero. When $\theta_{\text{os(a)}} = 0$, the nanostructures are impregnated by the lubricant with encapsulated features for the interface outside the droplet (interface C). When $0 < \theta_{\text{os(a)}} < \theta_c$, the nanostructures are impregnated by the lubricant but with emerging features. For the interface underneath the droplet (interface B), the nanostructures under the droplet could be impaled by water, impregnated by the lubricant with emergent features, or impregnated by the lubricant with encapsulated features with a correspondence of $\theta_{\text{os(w)}} > \theta_c$, $0 < \theta_{\text{os(w)}} < \theta_c$, and $\theta_{\text{os(w)}} = 0$, respectively. From Figure 4, we can see that the computational results are in good agreement with the theoretical solutions in ref 35, verifying the present numerical model.

However, the theoretical analysis³⁵ considered only the effects of surface wettability and interfacial tension. The lubricant thickness is given tacit consent enough to cover the nanostructures or to fully wrap the droplet. Still, this thickness might change in different applications and therefore influence

the morphology. Also, the effect of surface nanostructures is not yet clear. The lubricant thickness is hard to control and measure on such a small micrometer scale. The configuration of the lubricant on nanostructures is hard to observe and analyze. The contact angle of a droplet on the lubricant-impregnated surface can be measured, but the encapsulated state is hard to observe because of blocking by the oil. Under these circumstances, our numerical model could be a powerful tool for exploring the effects of the lubricant thickness, the surface geometry, the surface wettability, and the spreading coefficient on the morphology of this complicated four-component system.

Effect of the Lubricant Thickness. For the lubricant-impregnated surface, an important aspect is to understand how the working fluid interacts with the lubricant underneath and what modifications can lead to an extremely small sliding angle. Therefore, we do not study the interface outside the droplet (interface C) because the interface underneath the droplet (interface B) is the key factor influencing the droplet's moving behavior. From the analysis of the possible droplet morphologies, there are two possible configurations for interface B: encapsulated ($\epsilon_{\text{CT-Cu}} = 0.667$ kcal/mol and $\epsilon_{\text{W-Cu}} = 0.333$ kcal/mol, Figure 5a-i,ii) and emerged ($\epsilon_{\text{CT-Cu}} = 0.333$ kcal/mol and $\epsilon_{\text{W-Cu}} = 0.667$ kcal/mol, Figure 5a-iii,iv). In addition, the water droplet will be afloat on the lubricant under $\epsilon_{\text{CT-W}} = 0.35$ kcal/mol (cases 5a-i,iii) and will be in the cloaking state for $\epsilon_{\text{CT-W}} = 0.43$ kcal/mol (cases 5a-ii,iv). Therefore, there will be four combinations taking interfaces A and B into consideration. To explore the effect of the lubricant thickness, we apply different hexane bead numbers, N , changing from 0 to 640.

On the basis of the results shown in Figure 5a, we find that there are three more types of morphologies if taking the lubricant thickness into consideration compared to the theoretical predications. We give corresponding diagrams of every morphology to interpret, as shown in Figure 5b.

The first two rows in Figure 5 refer to the state in which nanostructures are encapsulated in the lubricant. When there is no lubricant, the droplet will be suspended in air on the nanostructures and form the superhydrophobic state. For the case that $\epsilon_{\text{CT-W}} = 0.35$ kcal/mol and when there are 128 hexane beads, the lubricant can fully cover the textures because $\theta_{\text{os(a)}} = 0$ for $\epsilon_{\text{CT-Cu}} = 0.667$ kcal/mol, but the gaps between textures are not fully filled by the lubricant. In this case, droplets will still be suspended on the surface. The droplet is affected by both the lubricant and the nanostructures, which is defined as state I as shown in Figure 5b. When the lubricant molecule number increases to 256, the lubricant can fully fill in the nanostructures. The droplet is, therefore, able to be fully supported and influenced by the lubricant. The nanostructures have the function of holding the lubricant and have nothing to do with the droplet. In the meantime, the lubricant is thin enough not to deform the droplet shape, and we defined this state as II. As the lubricant molecule number keeps increasing, the shape of the droplet is deformed by the thick lubricant but is still able to float on the lubricant, which is defined as state III. For case a-i, the droplets will always be afloat no matter what the thickness of the lubricant; the spreading coefficients are smaller than zero. For case a-ii, the first three states are the same as in case a-i. However, when the lubricant number reaches 640, the lubricant is thick enough to wrap the droplet and the droplet is in the cloaking state, which is defined as state IV. The third and fourth rows in Figure 5 refer to the state in which the nanostructures can emerge. When there is no lubricant, the droplet will wet and sink into the gaps between nanostructures. When $N = 128$ in case a-

Table 3. Energy Parameter Settings

parameter [kcal/mol]	$\theta_{\text{os(w)}} > \theta_c$	$0 < \theta_{\text{os(w)}} < \theta_c$	$\theta_{\text{os(w)}} = 0$
$\theta_{\text{os(a)}} = 0$	$\epsilon_{\text{CT-Cu}}$	0.333	0.667
	$\epsilon_{\text{W-Cu}}$	1.000	0.333
$0 < \theta_{\text{os(a)}} < \theta_c$	$\epsilon_{\text{CT-Cu}}$	0.185	0.185
	$\epsilon_{\text{W-Cu}}$	0.667	0.333
$\theta_{\text{os(a)}} > \theta_c$	$\epsilon_{\text{CT-Cu}}$	0.100	0.100
	$\epsilon_{\text{W-Cu}}$	0.667	0.333

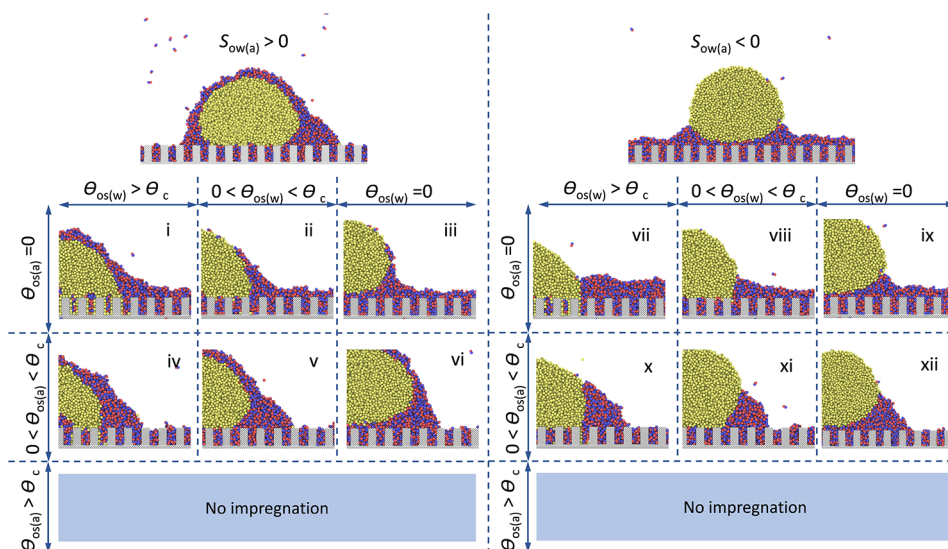


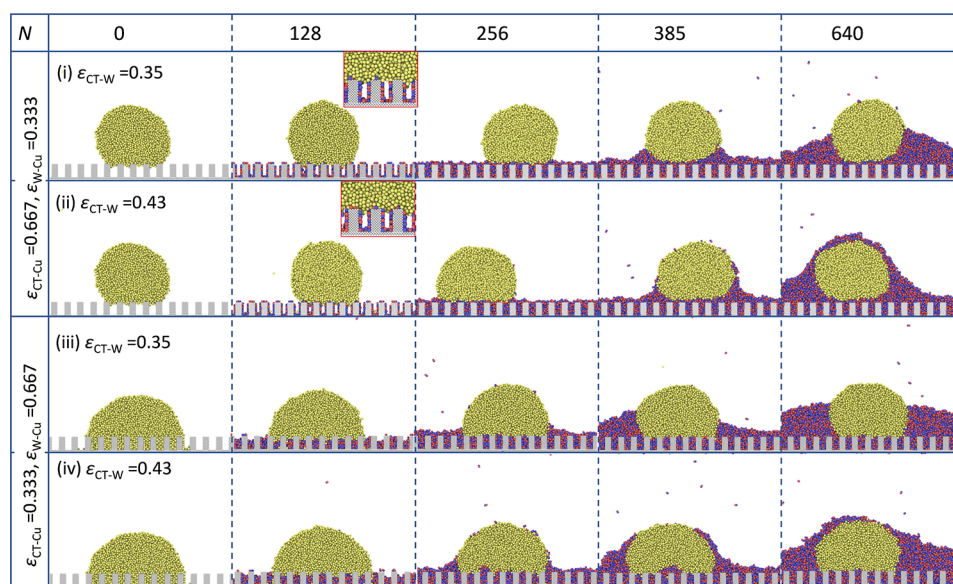
Figure 4. Possible thermodynamic states of a water nanodroplet placed on a lubricant-impregnated surface predicated by the simulation method. The top two schematics show whether the droplet gets cloaked by the lubricant. For each case, there are six possible states depending on how the lubricant wets the texture in the presence of air (the vertical axis) and water (horizontal axis). Snapshots with higher magnification are presented to show details of interfaces in this system. Parameters: (i) $\epsilon_{CT-W} = 0.43$, $\epsilon_{CT-Cu} = 0.333$, $\epsilon_{W-Cu} = 1.000$; (ii) $\epsilon_{CT-W} = 0.43$, $\epsilon_{CT-Cu} = 0.333$, $\epsilon_{W-Cu} = 0.667$; (iii) $\epsilon_{CT-W} = 0.43$, $\epsilon_{CT-Cu} = 0.667$, $\epsilon_{W-Cu} = 0.333$; (iv) $\epsilon_{CT-W} = 0.43$, $\epsilon_{CT-Cu} = 0.185$, $\epsilon_{W-Cu} = 0.667$; (v) $\epsilon_{CT-W} = 0.43$, $\epsilon_{CT-Cu} = 0.185$, $\epsilon_{W-Cu} = 0.333$; (vi) $\epsilon_{CT-W} = 0.43$, $\epsilon_{CT-Cu} = 0.185$, $\epsilon_{W-Cu} = 0.100$; (vii) $\epsilon_{CT-W} = 0.35$, $\epsilon_{CT-Cu} = 0.333$, $\epsilon_{W-Cu} = 1.000$; (viii) $\epsilon_{CT-W} = 0.35$, $\epsilon_{CT-Cu} = 0.333$, $\epsilon_{W-Cu} = 0.667$; (ix) $\epsilon_{CT-W} = 0.35$, $\epsilon_{CT-Cu} = 0.667$, $\epsilon_{W-Cu} = 0.333$; (x) $\epsilon_{CT-W} = 0.35$, $\epsilon_{CT-Cu} = 0.185$, $\epsilon_{W-Cu} = 0.667$; (xi) $\epsilon_{CT-W} = 0.35$, $\epsilon_{CT-Cu} = 0.185$, $\epsilon_{W-Cu} = 0.333$; and (xii) $\epsilon_{CT-W} = 0.35$, $\epsilon_{CT-Cu} = 0.185$, $\epsilon_{W-Cu} = 0.100$. Units: kcal/mol.

iii, the lubricant can fill gaps between nanostructures. The droplet is supported by the lubricant but can still touch the solid, which is defined as state V. When the number of lubricant molecules keeps increasing, the lubricant is thicker than the height of nanostructures. Wetting edges occur under this circumstance, but the interface beneath the droplet is still a composite solid and lubricant interface, which is defined as state VI. This state remains unchanged even when the lubricant number reaches 640. As for case a-iv, the droplet goes through states V and VI as the number of lubricant molecules increases, but when the lubricant is thick enough, the droplet will be cloaked in the lubricant, which is defined as state VII. Note that this state is different from state IV because the droplet in state VII can still touch the solid surface.

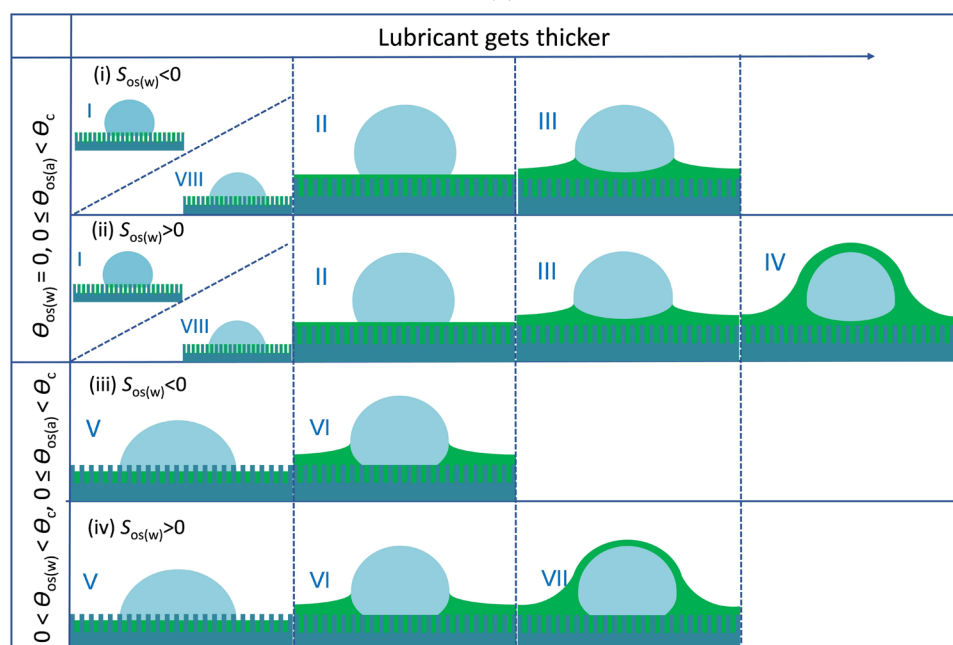
It should be noted that the wetting edge has an effect on the outlines of the droplet. For example, in the case of 640 lubricant molecules, the outlines of cases a and b can form small contact angle profiles. If we measure the contact angle as we do in an experiment, we might get the same contact angles for these three conditions, but we know from simulation results that the morphologies are quite different. Therefore, the contact angle on the SLIPS should be better marked with the corresponding lubricant thickness and parameters.

Effect of the Geometry of Nanostructures. We have demonstrated that the droplet morphology could be affected by the surface tension, the lubricant thickness, and the solid wettability. Next, we investigate the effect of surface nanostructures by changing the geometry of nanostructures. From the study above, it can be observed that the function of nanostructures is only to hold the lubricant after being fully covered by the lubricant. Therefore, if the geometry of surface nanostructures has any influence, it can happen only when the lubricant is thinner than the nanostructure height. For the cases when the nanostructures can emerge, the droplet will fill in the gaps between nanocolumns independently of the nanocolumn

width. The reason is that the parameters for the surface emergence will inevitably make the surface hydrophilic. The interfacial tension makes no difference when the lubricant thickness is small. Hence, we take only the condition for which nanostructures are in an encapsulated state into consideration, where $\epsilon_{CT-W} = 0.43$, $\epsilon_{CT-Cu} = 0.667$, and $\epsilon_{W-Cu} = 0.333$. The geometry used in the former study is defined as case a in Figure 6. A new geometry is constructed as case b in Figure 6 for comparison, where $a = 14.4596 \text{ \AA}$, $b = 49.1626 \text{ \AA}$, and $h = 32.5341 \text{ \AA}$. Accordingly, the critical angle in this geometry is 132.2° . The equilibrium states of droplets on these two different geometries infused with lubricants are shown in Figure 6. We also give the equilibrium state on the smooth surface (the first row in Figure 6) and the surface with nanostructures (the second row in Figure 6) as comparisons. With the same contact angle on the smooth surface, the droplet is in the Cassie state in case a but in the Wenzel state in case b when there is no lubricant. When the lubricant is thin and cannot fill up the gaps between nanostructures, the droplet of case a is in state I, as we describe in the droplet morphology analysis and show in Figure 5, in which the droplet is in the Cassie state with air beneath the droplet. In contrast, the droplet of case b is in the Wenzel state, where the water sinks into the gaps but also is supported by the lubricant and cannot touch the solid surface. The reason might be that the critical angle of case b is larger than that of case a with the same contact angle on a flat surface. When θ_c is larger than 120° , water droplets in the Wenzel state are more energetically favorable.⁵⁸ This state is different from state I and thus is defined as a new state, the corresponding diagram of which is added to Figure 5b and indicated as VIII. As the number of lubricant molecules keeps increasing, nanostructures can be fully covered, and the droplet morphologies are the same for these two different nanostructure geometries. The nanostructures have only the function of holding the lubricant and have nothing to do with the morphology.



(a)



(b)

Figure 5. (a) Morphologies under different lubricant numbers N and the following parameters: (i) $\epsilon_{CT-W} = 0.35$, $\epsilon_{CT-Cu} = 0.667$, $\epsilon_{W-Cu} = 0.333$, $\epsilon_{CT-W} = 0.35$; (ii) $\epsilon_{CT-W} = 0.43$, $\epsilon_{CT-Cu} = 0.667$, $\epsilon_{W-Cu} = 0.333$, $\epsilon_{CT-W} = 0.43$; (iii) $\epsilon_{CT-W} = 0.35$, $\epsilon_{CT-Cu} = 0.333$, $\epsilon_{W-Cu} = 0.667$, $\epsilon_{CT-W} = 0.35$; and (iv) $\epsilon_{CT-W} = 0.43$, $\epsilon_{CT-Cu} = 0.333$, $\epsilon_{W-Cu} = 0.667$, $\epsilon_{CT-W} = 0.43$. (b) Summary of possible morphologies on the lubricant-impregnated surface. The droplet will not be cloaked in cases i and iii and will be the cloaking state in cases ii and iv. The surface is encapsulated in the lubricant in cases i and ii and emerged in cases iii and iv. Snapshots with higher magnification are added to give gap details when necessary. Units: kcal/mol.

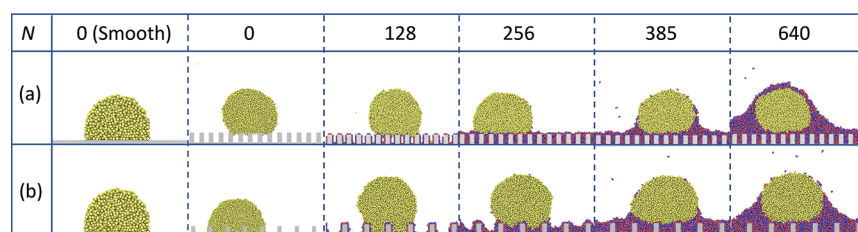


Figure 6. Morphologies of droplets on different nanostructures: $\epsilon_{CT-W} = 0.43$, $\epsilon_{CT-Cu} = 0.667$, and $\epsilon_{W-Cu} = 0.333$. Units: kcal/mol. (a) $a = 14.4596 \text{ \AA}$, $b = 17.3515 \text{ \AA}$, and $h = 32.5341 \text{ \AA}$. (b) $a = 14.4596 \text{ \AA}$, $b = 49.1626 \text{ \AA}$, and $h = 32.5341 \text{ \AA}$.

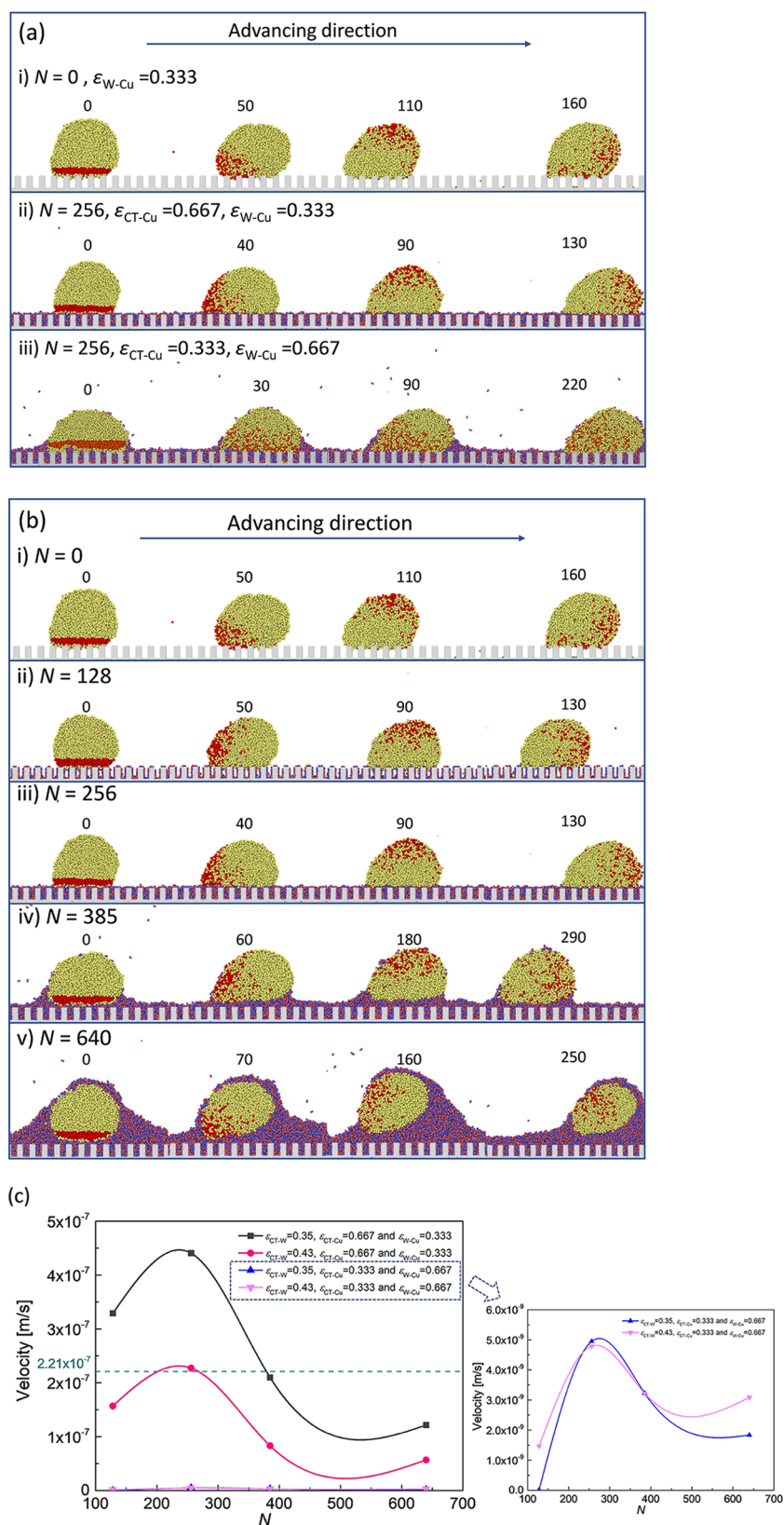


Figure 7. Droplet sliding behavior. (a) Side views to elucidate the mechanism of motion of water nanodroplets on SLIPS, $\epsilon_{CT-W} = 0.43$ kcal/mol. (b) Side view of water nanodroplet motion at different lubricant thicknesses, $\epsilon_{CT-W} = 0.43$ kcal/mol, $\epsilon_{CT-Cu} = 0.667$ kcal/mol, and $\epsilon_{W-Cu} = 0.333$ kcal/mol. (c) Average velocity as a function of lubricant numbers and energy parameters. The corresponding time of every snapshot is marked. Units: picoseconds.

In summary, we have extended the four possible primary morphologies existing on SLIPS to eight conditions. We believe

that this morphology exploration can be insightful and help us to determine the morphology of this complicated system and what

improvement could be useful in various applications for a given set of droplets, lubricant, and solid. For example, if the droplet is afloat on the lubricant, then changing the solid surface wettability has no influence on the droplet morphology. However, it might be useful for the cases in which nanostructures are in the emerged state, and droplets could touch the solid surface.

Droplet Dynamic Behavior on SLIPS. The most significant property of SLIPS is that the contact angle hysteresis is extremely small. Kim et al.⁶ reported that the contact angle hysteresis and the sliding speed of a water drop on SLIPS are significantly improved if an excess film is present. The lubricant characteristics will also have an influence on the droplet motion. Therefore, we explore the effects of the lubricant thickness and lubricant–water interfacial tension on the droplet dynamic behavior by comparing with the superhydrophobic surface. There are two mechanisms to consider when a droplet slides on SLIPS depending on whether the droplet can touch the solid (i.e., interface B is in the emerged ($\epsilon_{\text{CT-Cu}} = 0.667$ and $\epsilon_{\text{CT-W}} = 0.333$) or encapsulated ($\epsilon_{\text{CT-Cu}} = 0.333$ and $\epsilon_{\text{CT-W}} = 0.667$) state). With the consideration of interface A ($\epsilon_{\text{CT-W}} = 0.43$ or 0.35), there are four cases studied in this section.

To investigate the effect of interface B, we give a series of side views of water bead moving behavior on SLIPS, taking the case of $\epsilon_{\text{CT-W}} = 0.43$ and $N = 256$ as an example. The condition in which the number of lubricant molecules equals zero refers to the superhydrophobic surface (Figure 7a-i). The water droplets are able to move because a horizontal force is added to the initial equilibrium system. We color some water beads red to observe the motion trajectory. It is clearly observed that the water rotates when advancing for each case. The droplet moves smoothly on the lubricant surface when the droplet is fully supported by the lubricant (Figure 7a-ii). When the solid surface is in the emerged state, the droplet moves on the composite solid and lubricant surface (Figure 7a-iii). The contact angle changes because of the wettability difference between the solid part and the lubricant part. Next, we plot droplet motion behaviors under the effect of the lubricant thickness, as shown in Figure 7b, taking the case of $\epsilon_{\text{CT-W}} = 0.43$, $\epsilon_{\text{CT-Cu}} = 0.667$, and $\epsilon_{\text{W-Cu}} = 0.333$ as an example. The droplet moving process on the superhydrophobic surface where $N = 0$ is also plotted as a comparison. It can be seen that the droplet is able to roll and advance for all conditions, even when fully covered by the lubricant.

To quantitatively analyze the droplet moving behavior, we also calculated the droplet average velocity during 0.3 ns, which is plotted in Figure 7c. The horizontal line refers to the droplet average velocity on the superhydrophobic surface, where $N = 0$. For all four cases in Figure 7c, the velocity will increase at first as the number of lubricant molecules increases from 128 to 256 but decreases if the lubricant keeps increasing. These curves are consistent with the experimental results⁶ that the sliding speed of a water drop on SLIPS is significantly improved if an excess film is present, while the velocity gets smaller if the lubricant continues to increase. We think that there might be two factors influencing the droplet sliding velocity: the interfacial tension between water and copper/hexane and the surface roughness. When the number of lubricant molecules remains the same, the velocity corresponding to $\epsilon_{\text{CT-W}} = 0.43$ is smaller than that corresponding to $\epsilon_{\text{CT-W}} = 0.35$. Droplets slide faster when the interfacial tension is larger. When the number of hexane molecules is 128, compared to the superhydrophobic surface, the contact areas of water and lubricant are larger as a result of the coverage of hexane on the surface for cases a-i,ii. Along with a

relatively larger energy parameter of $\epsilon_{\text{CT-W}}(0.43)$, case a-ii has a smaller velocity than the superhydrophobic surface (represented by the dashed line). As for case a-i, the velocity is larger than that of the superhydrophobic surface despite the increased contact area, which might be the reason for the smaller energy parameter $\epsilon_{\text{CT-W}}(0.35)$. The droplet will get stuck in the excess lubricant film if the lubricant is too thick. A proper increase in the lubricant thickness might enhance the sliding velocity. It can also be seen that the droplet moves much slower (about 100 times slower) if touching the solid surface ($\epsilon_{\text{CT-Cu}} = 0.333$ and $\epsilon_{\text{W-Cu}} = 0.667$), compared to the case when the nanostructures are in the encapsulated state. The large energy parameter $\epsilon_{\text{W-Cu}}$ causes the droplet to be hard to move.

CONCLUSIONS

In this work, we have proposed a numerical model to analyze the lubricant-impregnated surface using the molecular dynamics simulations. We first proved the capability of this numerical method by showing the consistency of our simulation results against the previous theoretical studies. Furthermore, we have extended the four original possible stable states on SLIPS to eight states by considering the effects of the lubricant thickness and the surface geometry in addition to the interfacial tension and the surface wettability. The droplet dynamic behavior has been explored, and the influences of the lubricant thickness, the solid wettability, and the interfacial tension on the droplet sliding velocity have been investigated. It is suggested that a proper increase in the lubricant thickness might increase the sliding velocity for the encapsulated state of nanostructures. It is expected that the comprehensive analysis of stable states in this study can help to determine the morphology and what improvements could be useful in various applications for a given droplet, lubricant, and solid. The proposed numerical model could be applied to further studies under specific applications and provide design guidelines for the SLIPS.

ASSOCIATED CONTENT

Supporting Information

The Supporting Information is available free of charge at <https://pubs.acs.org/doi/10.1021/acs.langmuir.9b02603>.

Initial configurations of the water surface tension calculation, the hexane surface tension calculation, the water–hexane interfacial tension calculation, the water contact angle calculation in corresponding air, the hexane contact angle calculation in corresponding air, and the hexane contact angle calculation in water; steps to attain the equilibrium state of the water–hexane–copper system; sliding behavior calculation after equilibration; and contact angle of hexane in corresponding air $\theta_{\text{os(a)}}$ and water $\theta_{\text{os(w)}}$ under different energy parameter settings (PDF)

AUTHOR INFORMATION

Corresponding Authors

*E-mail: ghtag@mail.xjtu.edu.cn.

*E-mail: satish.kumar@me.gatech.edu.

ORCID

G. H. Tang: 0000-0002-7881-2573

Notes

The authors declare no competing financial interest.

ACKNOWLEDGMENTS

We gratefully acknowledge the funding from the National Natural Science Foundation of China under grant nos. 51825604 and 51576156 and the 111 Project under grant no. B16038. L.G. is also grateful for financial support from the China Scholarship Council.

REFERENCES

- (1) Riedel, M.; Eichner, A.; Jetter, R. Slippery surfaces of carnivorous plants: composition of epicuticular wax crystals in *Nepenthes alata* Blanco pitchers. *Planta* **2003**, *218* (1), 87–97.
- (2) Scholz, I.; Buckins, M.; Dolge, L.; Erlinghagen, T.; Weth, A.; Hischen, F.; Mayer, J.; Hoffmann, S.; Riederer, M.; Riedel, M.; Baumgartner, W. Slippery surfaces of pitcher plants: *Nepenthes* wax crystals minimize insect attachment via microscopic surface roughness. *J. Exp. Biol.* **2010**, *213* (7), 1115–1125.
- (3) Gorb, E. V.; Gorb, S. N. The effect of surface anisotropy in the slippery zone of *Nepenthes alata* pitchers on beetle attachment. *Beilstein J. Nanotechnol.* **2011**, *2*, 302–310.
- (4) Chen, H.; Zhang, P.; Zhang, L.; Liu, H.; Jiang, Y.; Zhang, D.; Han, Z.; Jiang, L. Continuous directional water transport on the peristome surface of *Nepenthes alata*. *Nature* **2016**, *532* (7597), 85–9.
- (5) Wong, T. S.; Kang, S. H.; Tang, S. K. Y.; Smythe, E. J.; Hatton, B. D.; Grinthal, A.; Aizenberg, J. Bioinspired self-repairing slippery surfaces with pressure-stable omniphobicity. *Nature* **2011**, *477* (7365), 443–447.
- (6) Kim, P.; Kreder, M. J.; Alvarenga, J.; Aizenberg, J. Hierarchical or not? Effect of the length scale and hierarchy of the surface roughness on omniphobicity of lubricant-infused substrates. *Nano Lett.* **2013**, *13* (4), 1793–1799.
- (7) Sunny, S.; Vogel, N.; Howell, C.; Vu, T. L.; Aizenberg, J. Lubricant-infused nanoparticle coatings assembled by layer-by-layer deposition. *Adv. Funct. Mater.* **2014**, *24* (42), 6658–6667.
- (8) Kreder, M. J.; Daniel, D.; Tetreault, A.; Cao, Z. L.; Lemaire, B.; Timonen, J. V. I.; Aizenberg, J. Film dynamics and lubricant depletion by droplets moving on lubricated surfaces. *Phys. Rev. X* **2018**, *8* (3), 031053.
- (9) Anand, S.; Paxson, A. T.; Dhiman, R.; Smith, J. D.; Varanasi, K. K. Enhanced condensation on lubricant-impregnated nanotextured surfaces. *ACS Nano* **2012**, *6* (11), 10122–10129.
- (10) Miljkovic, N.; et al. Condensation on hydrophilic, hydrophobic, nanostructured superhydrophobic and oil-infused surfaces. *J. Heat Transfer* **2013**, *135* (8), 080906.
- (11) Xiao, R.; Miljkovic, N.; Enright, R.; Wang, E. N. Immersion condensation on oil-infused heterogeneous surfaces for enhanced heat transfer. *Sci. Rep.* **2013**, *3*, 1988.
- (12) Rykaczewski, K.; Paxson, A. T.; Staymates, M.; Walker, M. L.; Sun, X. D.; Anand, S.; Srinivasan, S.; McKinley, G. H.; Chinn, J.; Scott, J. H. J.; Varanasi, K. K. Dropwise condensation of low surface tension fluids on omniphobic surfaces. *Sci. Rep.* **2015**, *4*, 4158.
- (13) Park, K. C.; Kim, P.; Grinthal, A.; He, N.; Fox, D.; Weaver, J. C.; Aizenberg, J. Condensation on slippery asymmetric bumps. *Nature* **2016**, *531* (7592), 78–82.
- (14) Kajiya, T.; Schellenberger, F.; Papadopoulos, P.; Vollmer, D.; Butt, H. J. 3D Imaging of water-drop condensation on hydrophobic and hydrophilic lubricant-impregnated surfaces. *Sci. Rep.* **2016**, *6*, 23687.
- (15) Tsuchiya, H.; Tenjimbayashi, M.; Moriya, T.; Yoshikawa, R.; Sasaki, K.; Togaawa, R.; Yamazaki, T.; Manabe, K.; Shiratori, S. Liquid-infused smooth surface for improved condensation heat transfer. *Langmuir* **2017**, *33* (36), 8950–8960.
- (16) Guo, L.; Tang, G. H. Dropwise condensation on bioinspired hydrophilic-slippy surface. *RSC Adv.* **2018**, *8*, 39341.
- (17) Epstein, A. K.; Wong, T. S.; Belisle, R. A.; Boggs, E. M.; Aizenberg, J. Liquid-infused structured surfaces with exceptional anti-biofouling performance. *Proc. Natl. Acad. Sci. U. S. A.* **2012**, *109* (33), 13182–13187.
- (18) Xiao, L. L.; Li, J. S.; Mieszkina, S.; Di Fino, A.; Clare, A. S.; Callow, M. E.; Callow, J. A.; Grunze, M.; Rosenhahn, A.; Levkin, P. A. Slippery liquid-infused porous surfaces showing marine antibiofouling properties. *ACS Appl. Mater. Interfaces* **2013**, *5* (20), 10074–10080.
- (19) Howell, C.; Vu, T. L.; Lin, J. J.; Kolle, S.; Juthani, N.; Watson, E.; Weaver, J. C.; Alvarenga, J.; Aizenberg, J. Self-replenishing vascularized fouling-release surfaces. *ACS Appl. Mater. Interfaces* **2014**, *6* (15), 13299–13307.
- (20) Wang, P.; Zhang, D.; Lu, Z. Slippery liquid-infused porous surface bio-inspired by pitcher plant for marine anti-biofouling application. *Colloids Surf., B* **2015**, *136*, 240–247.
- (21) MacCallum, N.; Howell, C.; Kim, P.; Sun, D.; Friedlander, R.; Ranisau, J.; Ahanotu, O.; Lin, J. J.; Vena, A.; Hatton, B.; Wong, T. S.; Aizenberg, J. Liquid-infused silicone as a biofouling-free medical material. *ACS Biomater. Sci. Eng.* **2015**, *1* (1), 43–51.
- (22) Sunny, S.; Cheng, G.; Daniel, D.; Lo, P.; Ochoa, S.; Howell, C.; Vogel, N.; Majid, A.; Aizenberg, J. Transparent antifouling material for improved operative field visibility in endoscopy. *Proc. Natl. Acad. Sci. U. S. A.* **2016**, *113* (42), 11676–11681.
- (23) Zhao, D.; Xu, X. D.; Yuan, S. S.; Yan, S. J.; Wang, X. H.; Luan, S. F.; Yin, J. H. Fouling-resistant behavior of liquid-infused porous slippery surfaces. *Chin. J. Polym. Sci.* **2017**, *35* (7), 887–896.
- (24) Kim, P.; Wong, T. S.; Alvarenga, J.; Kreder, M. J.; Adorno-Martinez, W. E.; Aizenberg, J. Liquid-infused nanostructured surfaces with extreme anti-ice and anti-frost performance. *ACS Nano* **2012**, *6* (8), 6569–6577.
- (25) Liu, Q.; Yang, Y.; Huang, M.; Zhou, Y. X.; Liu, Y. Y.; Liang, X. D. Durability of a lubricant-infused electrospray silicon rubber surface as an anti-icing coating. *Appl. Surf. Sci.* **2015**, *346*, 68–76.
- (26) Kreder, M. J.; Alvarenga, J.; Kim, P.; Aizenberg, J. Design of anti-icing surfaces: smooth, textured or slippery? *Nature Reviews Mater.* **2016**, *1* (1), 15003.
- (27) Yeong, Y. H.; Wang, C. Y.; Wynne, K. J.; Gupta, M. C. Oil-infused superhydrophobic silicone material for low ice adhesion with long-term infusion stability. *ACS Appl. Mater. Interfaces* **2016**, *8* (46), 32050–32059.
- (28) Rykaczewski, K.; Anand, S.; Subramanyam, S. B.; Varanasi, K. K. Mechanism of frost formation on lubricant-impregnated surfaces. *Langmuir* **2013**, *29* (17), 5230–5238.
- (29) Zhang, G. F.; Zhang, Q. H.; Cheng, T. T.; Zhan, X. L.; Chen, F. Q. Polyols-infused slippery surfaces based on magnetic Fe₃O₄-functionalized polymer hybrids for enhanced multifunctional anti-icing and deicing properties. *Langmuir* **2018**, *34* (13), 4052–4058.
- (30) Yu, C. M.; Zhu, X. B.; Li, K.; Cao, M. Y.; Jiang, L. Manipulating bubbles in aqueous environment via a lubricant-infused slippery surface. *Adv. Funct. Mater.* **2017**, *27*, 1701605.
- (31) Zhang, C. H.; Zhang, B.; Ma, H. Y.; Li, Z.; Xiao, X.; Zhang, Y. H.; Cui, X. Y.; Yu, C. M.; Cao, M. Y.; Jiang, L. Bioinspired pressure-tolerant asymmetric slippery surface for continuous self-transport of gas bubbles in aqueous environment. *ACS Nano* **2018**, *12* (2), 2048–2055.
- (32) Yousaf, M. R.; Yilbas, B. S.; Ali, H. Assessment of optical transmittance of oil impregnated and non-wetted surfaces in outdoor environment towards solar energy harvesting. *Sol. Energy* **2018**, *163*, 25–31.
- (33) Yong, J. L.; Huo, J. L.; Yang, Q.; Chen, F.; Fang, Y.; Wu, X. J.; Liu, L.; Lu, X. Y.; Zhang, J. Z.; Hou, X. Femtosecond laser direct writing of porous network microstructures for fabricating super-slippy surfaces with excellent liquid repellence and anti-cell proliferation. *Adv. Mater. Interfaces* **2018**, *5*, 1701479.
- (34) Lafuma, A.; Quere, D. Slippery pre-suffused surfaces. *EPL* **2011**, *96*, 56001.
- (35) Smith, J. D.; Dhiman, R.; Anand, S.; Reza-Garduno, E.; Cohen, R. E.; McKinley, G. H.; Varanasi, K. K. Droplet mobility on lubricant-impregnated surfaces. *Soft Matter* **2013**, *9* (6), 1772–1780.
- (36) Ma, W.; Higaki, Y.; Otsuka, H.; Takahara, A. Perfluoropolyether-infused nano-texture: a versatile approach to omniphobic coatings with low hysteresis and high transparency. *Chem. Commun.* **2013**, *49* (6), 597–599.
- (37) Wang, P.; Zhang, D.; Sun, S. M.; Li, T. P.; Sun, Y. Fabrication of slippery lubricant-infused porous surface with high underwater

transparency for the control of marine biofouling. *ACS Appl. Mater. Interfaces* **2017**, *9* (1), 972–982.

(38) Okada, I.; Shiratori, S. High-transparency, self-standable gel-SLIPS fabricated by a facile nanoscale phase separation. *ACS Appl. Mater. Interfaces* **2014**, *6* (3), 1502–1508.

(39) Yuan, S.; Li, Z.; Song, L.; Shi, H.; Luan, S.; Yin, J. Liquid-infused poly(styrene-*b*-isobutylene-*b*-styrene) microfiber coating prevents bacterial attachment and thrombosis. *ACS Appl. Mater. Interfaces* **2016**, *8* (33), 21214–21220.

(40) Wang, J.; Kato, K.; Blois, A. P.; Wong, T. S. Bioinspired omniphobic coatings with a thermal self-repair function on industrial materials. *ACS Appl. Mater. Interfaces* **2016**, *8* (12), 8265–8271.

(41) Nishioka, S.; Tenjimayashi, M.; Manabe, K.; Matsubayashi, T.; Suwabe, K.; Tsukada, K.; Shiratori, S. Facile design of plant-oil-infused fine surface asperity for transparent blood-repelling endoscope lens. *RSC Adv.* **2016**, *6* (53), 47579–47587.

(42) Anand, S.; Rykaczewski, K.; Subramanyam, S. B.; Beysens, D.; Varanasi, K. K. How droplets nucleate and grow on liquids and liquid impregnated surfaces. *Soft Matter* **2015**, *11* (1), 69–80.

(43) Schellenberger, F.; Xie, J.; Encinas, N.; Hardy, A.; Klapper, M.; Papadopoulos, P.; Butt, H. J.; Vollmer, D. Direct observation of drops on slippery lubricant-infused surfaces. *Soft Matter* **2015**, *11* (38), 7617–7626.

(44) Subramanyam, S. B.; Rykaczewski, K.; Varanasi, K. K. Ice adhesion on lubricant-impregnated textured surfaces. *Langmuir* **2013**, *29* (44), 13414–13418.

(45) Kajiya, T.; Schellenberger, F.; Papadopoulos, P.; Vollmer, D.; Butt, H. J. 3D imaging of water-drop condensation on hydrophobic and hydrophilic lubricant-impregnated surfaces. *Sci. Rep.* **2016**, *6*, 23687.

(46) You, I.; Lee, T. G.; Nam, Y. S.; Lee, H. Fabrication of a micro-omnifluidic device by omniphilic/omniphobic patterning on nanostructured surfaces. *ACS Nano* **2014**, *8* (9), 9016–9024.

(47) Guan, J. H.; Wells, G. G.; Xu, B.; McHale, G.; Wood, D.; Martin, J.; Stuart-Cole, S. Evaporation of sessile droplets on slippery liquid-infused porous surface (SLIPS). *Langmuir* **2015**, *31*, 11781–11789.

(48) Ramos-Alvarado, B.; Kumar, S.; Peterson, G. P. Wettability of graphitic-carbon and silicon surfaces: MD modeling and theoretical analysis. *J. Chem. Phys.* **2015**, *143* (4), 044703.

(49) Xu, W.; Lan, Z.; Peng, B. L.; Wen, R. F.; Ma, X. H. Effect of surface free energies on the heterogeneous nucleation of water droplet: a molecular dynamics simulation approach. *J. Chem. Phys.* **2015**, *142* (5), 054701.

(50) Li, L.; Ji, P.; Zhang, Y. Molecular dynamics simulation of condensation on nanostructured surface in a confined space. *Appl. Phys. A: Mater. Sci. Process.* **2016**, *122*, 496.

(51) Niu, D.; Tang, G. H. The effect of surface wettability on water vapor condensation in nanoscale. *Sci. Rep.* **2016**, *6*, 19192.

(52) Gao, S.; Liao, Q.; Liu, W.; Liu, Z. Effects of solid fraction on droplet wetting and vapor condensation: a molecular dynamic simulation study. *Langmuir* **2017**, *33* (43), 12379–12388.

(53) Chiu, S. W.; Scott, H. L.; Jakobsson, E. A coarse-grained model based on Morse potential for water and *n*-alkanes. *J. Chem. Theory Comput.* **2010**, *6* (3), 851–863.

(54) Shinoda, W.; DeVane, R.; Klein, M. L. Multi-property fitting and parameterization of a coarse grained model for aqueous surfactants. *Mol. Simul.* **2007**, *33* (1–2), 27–36.

(55) Marrink, S. J.; de Vries, A. H.; Mark, A. E. Coarse grained model for semiquantitative lipid simulations. *J. Phys. Chem. B* **2004**, *108* (2), 750–760.

(56) Weijs, J. H.; Marchand, A.; Andreotti, B.; Lohse, D.; Snoeijer, J. H. Origin of line tension for a Lennard-Jones nanodroplet. *Phys. Fluids* **2011**, *23*, 022001.

(57) Lafuma, A.; Quere, D. Superhydrophobic states. *Nat. Mater.* **2003**, *2* (7), 457–60.

(58) Dai, X. M.; Stogin, B. B.; Yang, S. K.; Wong, T. S. Slippery Wenzel state. *ACS Nano* **2015**, *9* (9), 9260–9267.

■ NOTE ADDED AFTER ASAP PUBLICATION

This article was published ASAP on November 21, 2019. An update was made to the caption of Figure 6 and to corresponding text in the Effect of the Geometry of Nanostructures section. The corrected version was reposted on December 2, 2019.